Gamma band activity in the developing parafascicular nucleus

Nebojsa Kezunovic, James Hyde, Christen Simon, Francisco J. Urbano, D. Keith Williams and Edgar Garcia-Rill

You might find this additional info useful...

Updated information and services including high resolution figures, can be found at:
http://jn.physiology.org/content/107/3/772.full.html

Additional material and information about *Journal of Neurophysiology* can be found at:
http://www.the-aps.org/publications/jn

This infomation is current as of January 25, 2012.

Gamma band activity in the developing parafascicular nucleus

Nebojsa Kezunovic,[1] James Hyde,[1] Christen Simon,[1] Francisco J. Urbano,[2] D. Keith Williams,[1] and Edgar Garcia-Rill[1]

[1]*Center for Translational Neuroscience, Departments of Neurobiology and Developmental Sciences and Biometry, University of Arkansas for Medical Sciences, Little Rock, Arkansas; and* [2]*Instituto de Fisiología, Biología Molecular y Neurociencias, Consejo Nacional de Investigaciones Científicas y Técnicas, University of Buenos Aires, Buenos Aires, Argentina*

Kezunovic N, Hyde J, Simon C, Urbano FJ, Williams DK, Garcia-Rill E. Gamma band activity in the developing parafascicular nucleus. *J Neurophysiol* 107: 772–784, 2012. First published November 16, 2011; doi:10.1152/jn.00677.2011.—The parafascicular nucleus (Pf) receives cholinergic input from the pedunculopontine nucleus, part of the reticular activating system involved in waking and rapid eye movement (REM) sleep, and sends projections to the cortex. We tested the hypothesis that Pf neurons fire maximally at gamma band frequency (30–90 Hz), that this mechanism involves high-threshold voltage-dependent P/Q- and N-type calcium channels, and that this activity is enhanced by the cholinergic agonist carbachol (CAR). Patch-clamped 9- to 25-day-old rat Pf neurons ($n = 299$) manifested a firing frequency plateau at gamma band when maximally activated (31.5 ± 1.5 Hz) and showed gamma oscillations when voltage-clamped at holding potentials above -20 mV, and the frequency of the oscillations increased significantly with age (24.6 ± 3.8 vs. 51.6 ± 4.4 Hz, $P < 0.001$) but plateaued at gamma frequencies. Cells exposed to CAR showed significantly higher frequencies early in development compared with those without CAR (24.6 ± 3.8 vs. 41.7 ± 4.3 Hz, $P < 0.001$) but plateaued with age. The P/Q-type calcium channel blocker ω-agatoxin-IVA (ω-Aga) blocked gamma oscillations, whereas the N-type blocker ω-conotoxin-GVIA (ω-CgTx) only partially decreased the power spectrum amplitude of gamma oscillations. The blocking effect of ω-Aga on P/Q-type currents and ω-CgTx on N-type currents was consistent over age. We conclude that P/Q- and N-type calcium channels appear to mediate Pf gamma oscillations during development. We hypothesize that the cholinergic input to the Pf could activate these cells to oscillate at gamma frequency, and perhaps relay these rhythms to cortical areas, thus providing a stable high-frequency state for "nonspecific" thalamocortical processing.

ω-agatoxin IVA; arousal; carbachol; calcium currents; ω-conotoxin-GVIA; gamma oscillations

THE PARAFASCICULAR NUCLEUS (Pf) is a component of the intralaminar thalamus (ILT), part of the "nonspecific" thalamocortical system. Pf neurons send widespread projections to the cortex, striatum, subthalamic nucleus, and substantia nigra (Herrero et al. 2002; Van der Werf et al. 2002). The Pf is thought to be involved in maintaining consciousness and selective attention in primates (Minamimoto and Kimura 2002; Raeva 2006). Electrical stimulation of the centrolateral (CL)-Pf nuclei in vivo is known to produce arousal and gamma band activity in the cortical EEG (Steriade and Demetrescu 1960). However, little is known about the intrinsic properties of Pf

neurons, as well as the role of the Pf in the "nonspecific" thalamocortical system.

During the activated states of waking and rapid eye movement (REM) sleep, EEG recordings are characterized by low-amplitude, high-frequency oscillatory activity in the gamma band range ($\sim$30–90 Hz). We recently reported that, regardless of cell type, almost all pedunculopontine nucleus (PPN) neurons fired at gamma band frequency, but no higher, when subjected to depolarizing steps (Simon et al. 2010). We also reported that PPN neurons, some of which are cholinergic, have intrinsic membrane properties that allow them to oscillate at gamma band frequency through specific calcium and potassium channels (Kezunovic et al. 2011). The ILT receives projections from the cholinergic PPN and laterodorsal tegmental (LDT) nuclei with both symmetrical and asymmetrical terminals (Capozzo et al. 2003; Erro et al. 1999; Kha et al. 2000; Kobayashi and Nakamura 2003), which in turn may participate in the modulation of cortical arousal, attention, and sensory awareness (Minamimoto and Kimura 2002; Raeva 2006; Steriade and Demetrescu 1960). Cholinergic PPN neurons are most active during the activated, high-frequency EEG states of waking and REM sleep and contribute to the generation of fast thalamocortical oscillations (Steriade et al. 1990). Release of acetylcholine in the thalamus induced by PPN stimulation (Williams et al. 1994) blocks spindle oscillations and delta waves that appear in slow wave sleep (SWS), triggers the fast cortical oscillations of waking and REM sleep by depolarizing thalamocortical (TC) relay neurons in "specific" thalamic nuclei (McCormick 1992), and hyperpolarizes reticular thalamic neurons (nRt) (Hobson and Pace-Schott 2002; Steriade et al. 1993). Interestingly, the amount of REM sleep in rats decreases from about 75% of the total sleep time at *day 10* to about 15% at *day 30* (Jouvet-Mounier et al. 1970). Most of the changes in PPN transmitter interactions occur across the 12- to 16-day period (reviewed in Garcia-Rill et al. 2008).

Voltage-gated calcium channels play a pivotal role in determining intrinsic membrane properties and in modulating synaptic transmission (Caterall 1998; Katz and Miledi 1965; Llinas 1988; Llinas and Hess 1976). High-threshold P/Q-type channels are known to be located in the dendrites of "specific" TC relay neurons and support gamma band oscillations in the thalamus (Luo and Perkel 1999; Pedroarena and Llinas 1997; Rhodes and Llinas 2005), as well as at cortical levels (Jones 2007; Llinas et al. 2007). However, it is not clear whether "nonspecific" or ILT neurons, whose intrinsic properties differ considerably from those of "specific" TC relay cells (Phelan et al. 2005), exhibit gamma band activity. N-type calcium channels ($Ca_V 2.2$) are found on presynaptic terminals throughout

the brain and peripheral nervous system. N-type calcium channel-deficient animals exhibit deficits in long-term potentiation and long-term memory (Jeon et al. 2007). Another important calcium channel is the low-threshold voltage-gated T-type calcium channel ($Ca_V 3.1–3.3$), which plays a role in synaptic integration (Nelson et al. 2006). In the Pf, T-type calcium channels mediate low-threshold spikes (LTS) (Beatty et al. 2009; Phelan et al. 2005, Ye et al. 2009). However, the role of Pf intrinsic properties, in particular P/Q- and N-type calcium channels, in the generation of gamma band activity is unknown. The present study was carried out to determine the mechanism(s) behind the manifestation of gamma band activity in single Pf neurons.

METHODS

Slice preparation. All experimental protocols were approved by the Institutional Animal Care and Use Committee of the University of Arkansas for Medical Sciences and were in agreement with the National Institutes of Health guidelines for the care and use of laboratory animals. Rat pups aged 9–25 days from adult timed-pregnant Sprague-Dawley rats (280–350 g) were anesthetized with ketamine (70 mg/kg im) until tail pinch reflex was absent. This age range was selected due to the developmental decrease in REM sleep in the rat that occurs between 10 and 30 days (Jouvet-Mounier et al. 1970). Most of the changes in PPN transmitter interactions occur across the period from 12 to 16 days (reviewed in Garcia-Rill et al. 2008). The period of investigation selected enabled us to study the age-related changes in the properties described below. Pups were decapitated, and the brain was rapidly removed and cooled in oxygenated sucrose-artificial cerebrospinal fluid (sucrose-aCSF). The sucrose-aCSF consisted of (in mM) 233.7 sucrose, 26 $NaHCO_3$, 3 KCl, 8 $MgCl_2$, 0.5 $CaCl_2$, 20 glucose, 0.4 ascorbic acid, and 2 sodium pyruvate. Sagittal sections (400 μm) containing the Pf nucleus were cut, and slices were allowed to equilibrate in normal aCSF at room temperature for 1 h before recording. The aCSF was composed of (in mM) 117 NaCl, 4.7 KCl, 1.2 $MgCl_2$, 2.5 $CaCl_2$, 1.2 NaH_2PO_4, 24.9 $NaHCO_3$, and 11.5 glucose. Slices were recorded at 37°C while perfused (1.5 ml/min) with oxygenated aCSF (95% O_2-5% CO_2) in an immersion chamber containing the following synaptic receptor antagonists: the selective NMDA receptor antagonist 2-amino-5-phosphonovaleric acid (APV; 40 μM), the competitive AMPA/kainate glutamate receptor antagonist 6-cyano-7-nitroquinoxaline-2,3-dione (CNQX; 10 μM), the glycine receptor antagonist strychnine (STR; 10 μM), and the specific $GABA_A$ receptor antagonist gabazine (GBZ; 10 μM).

Whole cell patch-clamp recordings. Differential interference contrast optics were used to visualize neurons with the use of an upright microscope (Nikon FN-1; Nikon). Whole cell recordings were performed using borosilicate capillary glass tubing pulled on a P-97 puller (Sutter Instrument, Novato, CA). During action potential (AP) studies, electrodes were filled with intracellular solution containing (in mM) 124 K-gluconate, 10 HEPES, 10 phosphocreatine di(tris), 0.2 EGTA, 4 Mg_2ATP, and 0.3 Na_2GTP. Experiments studying the oscillatory behavior of Pf neurons used high-K^+ intracellular solution containing (in mM) 10 phosphocreatine, 10 HEPES, 1 EGTA, 4 Mg-ATP, 0.4 Na_2GTP, 130 $KMeSO_3$, 10 NaCl, 2 $MgCl_2$, and 10 sucrose. To study calcium currents, electrodes were filled with high-Cs^+/QX-314 intracellular solution containing (in mM) 110 $CsMeSO_3$, 40 HEPES, 1 EGTA, 5 QX-314, 10 tetraethylammonium-Cl, 4 Mg-ATP, 0.4 Na_2GTP, 10 phosphocreatine, and 2 $MgCl_2$. Cesium is a widely used potassium channel blocker, whereas QX-314 blocks sodium channels intracellularly. Osmolarity was adjusted to ~270–290 mosM and pH to 7.3. The pipette resistance was 2–4 MΩ. All recordings were made using a Multiclamp 700B amplifier (Molecular Devices, Sunnyvale, CA) in both current- and voltage-clamp mode.

Analog signals were low-pass filtered at 2 kHz and digitized at 5 kHz with the use of a Digidata-1440A interface and pClamp10 software (Molecular Devices). The recording region was located immediately anterior and posterior to the middle third of the fasciculus retroflexus. Gigaseal and further access to the intracellular neuronal compartment were achieved in voltage-clamp mode, with the holding potential set at −50 mV (i.e., near the average resting membrane potential of Pf neurons). Soon after the membrane was ruptured, the intracellular solution reached equilibrium with the pipette solution without significant changes in either series resistance or membrane capacitance values. To study the maximal firing frequency of APs in Pf neurons, we used 500-ms depolarizing pulses, in 20-pA steps, in current-clamp mode. Presumed calcium-mediated oscillatory activity of Pf neurons was studied in both voltage-clamp and current-clamp modes, in the presence of synaptic blockers (see above) and tetrodotoxin (TTX; 3 μM). Membrane voltage was depolarized from the −50-mV holding potential to 0 mV, in 5-mV steps, without compensating series resistance (range 5–12 MΩ). The configuration was then changed to current-clamp mode, and the membrane potential was then depolarized using either 1-s duration square or ramp current protocols. No significant rundown due to intracellular dialysis of Pf neuron supra- or subthreshold activity was observed during our recording period (up to 40 min). Voltage-dependent calcium currents were studied using the high-Cs^+/QX-314 pipette solution, also in the presence of synaptic blockers and TTX. Either square-wave voltage steps or voltage ramps were used to generate Pf neuronal calcium currents. Fast compensation was used to maintain the series resistance values <10 MΩ.

For histological purposes, some recordings were conducted with 0.2% Lucifer yellow in the intracellular solution. Slices were fixed with 4% paraformaldehyde and visualized with a Nikon AZ100 epifluorescence microscope.
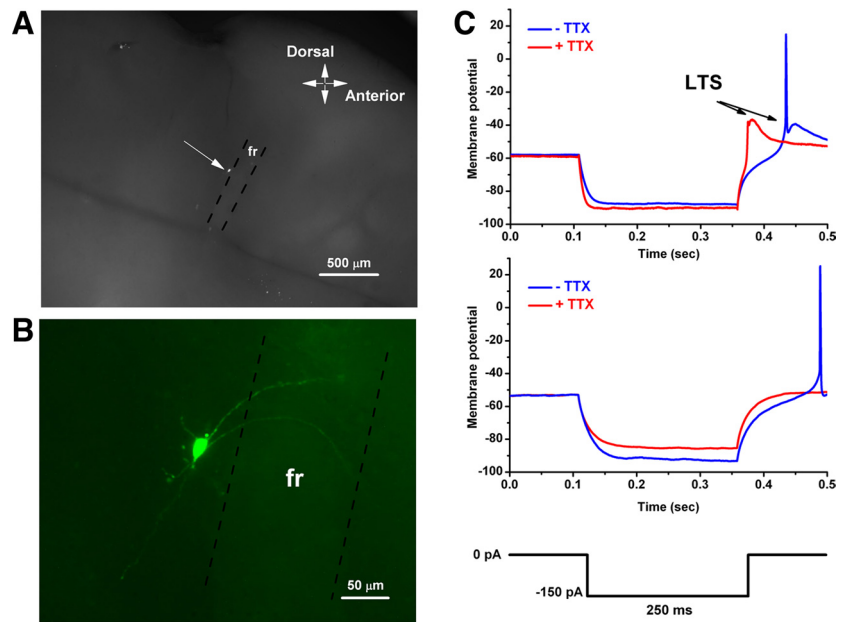
Drug application. Bath-applied drugs were administered to the slice via a peristaltic pump (Cole-Parmer, Vernon Hills, IL) and a three-way valve system such that solutions reached the slice 1.5 min after the start of application. The sodium channel blocker tetrodotoxin citrate (TTX; 3 μM) was purchased from Sigma (St. Louis, MO), as well as the cholinergic agonist carbachol (CAR; 30 μM). CAR was applied to the extracellular solution, containing fast synaptic blockers and TTX, 20 min before the recording. We wanted to study the effect of CAR in the steady-state condition; therefore, we allowed CAR to diffuse throughout the slice (15–20 min) before recording. The calcium channel blockers were purchased from either Peptide International (http://pepnet.com) or Alomone Labs (http://alomone.com). We used ω-agatoxin-IVA (ω-Aga; 200 nM), a specific P/Q-type calcium channel blocker, and ω-conotoxin-GVIA (ω-CgTx; 2.5 μM), a specific N-type calcium channel blocker, to confirm the calcium channel subtypes mediating both gamma oscillations and calcium currents.

Data analysis. Off-line analyses were performed using Clampfit software (Molecular Devices). Comparisons between groups were carried out using either Student's *t*-test or one-way ANOVA, with Bonferroni post hoc testing for multiple comparisons. A repeated-measures ANOVA model was fit for each response using SAS Proc Mixed software (SAS Institute, Cary, NC), and the Bonferroni test was again employed to control for multiple comparisons. Both *t* values and degrees of freedom (df) are reported for all linear regression ANOVAs. Differences were considered significant at values of $P \leq 0.05$. All results are presented as means ± SE.

RESULTS

Whole cell patch-clamp recordings were performed on a total of 299 Pf neurons, localized as previously described (Ye et al. 2009). The cells were recorded immediately anterior or posterior to the middle third of the fasciculus retroflexus, which are easily identified in sagittal sections (Fig. 1, *A* and *B*). Without exception, all cells were spindle-shaped with bipolar dendrites as previously described (Ye et al. 2009). We did not

Fig. 1. Localization and morphology of parafascicular (Pf) neurons. *A*: location (arrow) of a single recorded neuron (13 days old) immediately posterior to the fasciculus retroflexus (fr) in a 400-μm parasagittal thalamic section (bright field image). *B*: wide-field fluorescence image of the same neuron identified by intracellular 0.2% Lucifer yellow. Note the long, sparsely branching processes. *C*: examples of 150-pA (250 ms) hyperpolarizing pulses recorded in every Pf neuron used to identify the presence (*top* records) or absence (*bottom* records) of low-threshold spike (LTS) currents in the presence (red records) or absence (blue records) of tetrodotoxin (TTX). The morphology of the cells with or without LTS currents was similar.

sample more laterally located cells with bushy dendrites (more easily seen in coronal sections) because some authors believe they are part of the CL (Beatty et al. 2009), and their appearance is closer to that of "specific" thalamic neurons. We first identified Pf neurons according to the presence or absence of LTS currents by using hyperpolarizing current steps (Fig. 1*C*), as previously reported (Phelan et al. 2005; Ye et al. 2009). No difference in the average resting membrane potential was observed between cells with (+LTS) or without (−LTS) these currents (+LTS: 57.1 ± 1 mV, *n* = 35; −LTS: 56.3 ± 1.4 mV, *n* = 18; 1-way ANOVA, *P* = 0.44). We then studied the firing frequency of Pf neurons during depolarizing steps in the presence of fast synaptic blockers (APV, 40 μM; CNQX, 10 μM; STR, 10 μM; and GBZ, 10 μM). This study was followed by investigation of the effects of current ramps on membrane oscillatory properties in the presence of fast synaptic blockers and TTX. Because Pf neurons receive cholinergic input from mesopontine nuclei, we also studied the effects of CAR on membrane oscillatory properties. Finally, we pharmacologically characterized the channel types responsible for the generation of these oscillations.

Firing properties of Pf neurons. To determine the maximal firing frequency of Pf neuron APs, we used steps of increasing current amplitudes in current-clamp mode. This protocol applied nine 500-ms-duration current steps with an increase of 20 pA for each step and a 10-s interstep interval up to the final step of 180 pA (Fig. 2, *A* and *B*). During the current steps, neurons were depolarized and fired APs when above AP threshold. We measured the interspike intervals (ISI) between the first two, the middle two (~250 ms from the beginning of the step), and the last two APs during each current step and converted them to frequency (Fig. 2, *A* and *B*). In addition, the average firing frequency during the entire step was calculated. All Pf neurons had a characteristic pattern of firing during specific depolarizing steps. The 140-pA step is an example of the induced firing frequency using higher current steps (Fig. 2*A*) and also marks the beginning of the plateau effect on firing frequency. Note the shorter ISIs at the beginning compared with the middle or the end of the depolarizing step. We also analyzed other

characteristics of Pf neurons (AP amplitude, AP half-width, input resistance, and resting membrane potential), which were similar to those previously reported (Ye et al. 2009) (see Table 1).

A graph of the average AP firing frequency during the beginning (filled square), middle (filled circle), and end (filled triangle) of each current step was generated for all Pf neurons (*n* = 35) included in this particular experiment (Fig. 2*B*). The AP firing frequency increased with increasing amplitude current steps. However, the firing frequency plateaued at gamma frequency, and no higher, during the higher amplitude depolarizing steps (140–180 pA). At the 180-pA step, the cells fired at 46.2 ± 2.4 Hz at the beginning of the step. After this initial peak in firing frequency, the firing rate of these neurons decreased during the middle and at the end of the stimulus, but the firing rate remained within the beta/gamma range (24.8 ± 0.9 Hz for the middle ISI and 22.5 ± 0.8 Hz for the last ISI). The average overall firing frequency throughout the 180-pA step was in the gamma range (35.1 ± 1.5 Hz). One-way ANOVA was performed to compare the firing frequency at different steps with that at baseline (spontaneous APs at the resting membrane potential showed an average frequency of 0.9 ± 0.3 Hz; note that most cells did not show spontaneous activity, so this mean is for only those that did show some activity, *n* = 2). Statistical significance was found across all the ISIs at all depolarizing steps (*P* < 0.05).

In our previous study on the firing properties of PPN neurons (Simon et al. 2010), we showed that some cells accommodated at very high depolarizing steps (maximal step 270 pA). Their APs were significantly reduced in amplitude or completely disappeared and were replaced by small-amplitude oscillatory activity. In this study, we observed the same phenomenon (Fig. 2*C*, *middle* record) using five pyramidally arranged depolarizing steps (50, 150, 500, 150, and 50 pA) applied 10 s apart in another group of cells (*n* = 19). The second step (150 pA) was in the same current amplitude range as the depolarizing steps shown in Fig. 2*A* (140 pA). The firing frequency at these steps was characteristic of the firing pattern of Pf neurons observed in the group of cells described above using nine current steps. However, during the middle step (500 pA), the APs were
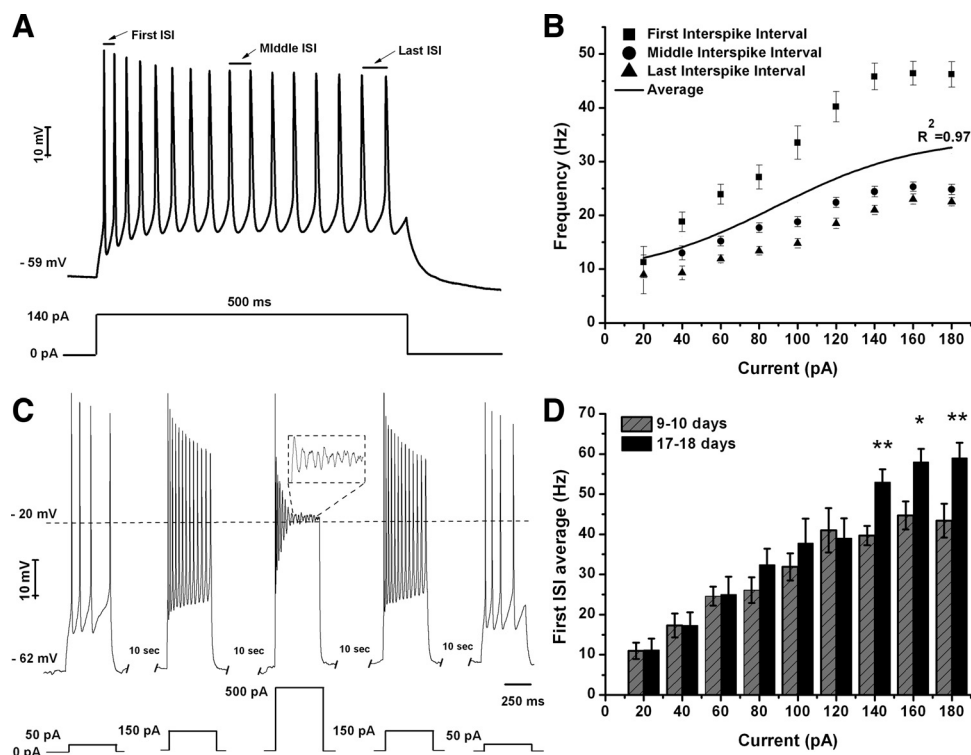
Fig. 2. Gamma band activity in whole cell recorded Pf neurons. *A*: maximal action potential (AP) frequency was measured using 9 current steps (each step was 500 ms in duration with an increase of 20 pA per step, with the last step at 180 pA and a 10-s delay between steps). The record shown in *A* is a representative response to a 140-pA step. Note the locations of the first, middle, and last interspike intervals (ISI) used to analyze the firing frequency of all Pf neurons. *B*: graph showing the average of the first (■), middle (●), and last (▴) ISI (converted to frequency) of Pf neurons ($n = 35$, 9–18 days). The black line shows the average instantaneous firing frequency during the entire current step. Note that firing frequency did not increase linearly with increasing current during the last few steps (140–180 pA) but instead plateaued at gamma frequency. *C*: pyramidal depolarizing steps (5 steps 500 ms long and 10 s apart) with a 500-pA step in the middle showing APs being replaced by oscillations at the highest depolarizing level (magnified view in dashed square). Note that the firing frequency of the APs returned to the usual firing rate when lower amplitude current steps were used (150 and 50 pA, respectively). *D*: bar graph of the first ISI average firing frequency during depolarizing steps. Note that at higher amplitude depolarizing steps, older neurons (17–18 days, black bars) fired faster than the younger ones (9–10 days, gray hatched bars). *$P < 0.05$; **$P < 0.01$.

almost abolished, except for the one at the beginning of the step. Interestingly, this high level of depolarization revealed oscillatory activity during the rest of the step similar to that previously reported in the PPN (Simon et al. 2010). A magnified view of these oscillations is shown in the *inset* above the *middle* step of Fig. 2*C*. Importantly, the descending-amplitude depolarizing steps (150 and 50 pA, respectively) revealed that Pf neurons again manifested normal APs and firing frequency, suggesting that the high level of depolarization had not killed or damaged the cells. All Pf neurons used in this five-step experiment showed the same characteristics of firing ($n = 19$).

Finally, the firing frequency of APs was compared across age groups (Fig. 2*D*). One-way ANOVA was used to compare 9- to 12-day-old cells with 17- to 25-day-old cells. Statistical

analysis revealed that the first ISIs of the 17- to 18-day-old group at 140-pA (53 ± 3.2 Hz, $P < 0.01$), 160-pA (58 ± 3.3 Hz, $P < 0.05$), and 180-pA steps (59 ± 3.8 Hz, $P < 0.01$) showed significantly higher firing rates compared with the 9- to 10-day-old group (140 pA: 40 ± 2.4 Hz; 160 pA: 45 ± 3.5 Hz; 180 pA: 43 ± 4.2 Hz). Interestingly, no statistical significance was found for the middle and the last ISIs between these two age groups. Also, there was no statistically significant difference in the AP mean frequencies between cells at 9–12 vs. 13–16 vs. 17–25 days (data not shown).

Depolarizing ramps generated gamma band oscillations in all Pf neurons in the presence of TTX. We tested the hypothesis that, in the presence of fast synaptic blockers and TTX, the remaining oscillatory activity observed in Pf neurons during current-clamp square-pulse depolarization was due to the activation of voltage-dependent calcium channels. Because of the extensive and rapid activation of potassium channels during depolarization, Pf neurons could not be depolarized beyond −20 mV by using current steps. Therefore, we chose to use 1-s-long depolarizing current ramps to gradually change the membrane potential from resting values up to 0 mV. In the presence of fast synaptic blockers and TTX (see METHODS), square pulses generated smaller amplitude (and power of) oscillations (Fig. 3, *A* and *B*, red records) compared with the amplitude and power of the oscillations generated by current

Table 1. *Properties of Pf neurons recorded during different ages*

	P9–12	P13–16	P17–18
n	13	15	7
Resting membrane potential, mV	−63.2 ± 1.8	−65.4 ± 1.8	−57.6 ± 2.7
Input resistance, MΩ	237 ± 22.8	184 ± 13.4	199 ± 24.7
Action potential amplitude, mV	57.2 ± 1.2	56.2 ± 1.1	58.7 ± 1.7
Action potential half-width, ms	2.1 ± 0.2	2.1 ± 0.3	1.6 ± 0.2

Values are means ± SE; age of parafascicular (Pf) neurons is given in postnatal days (P).
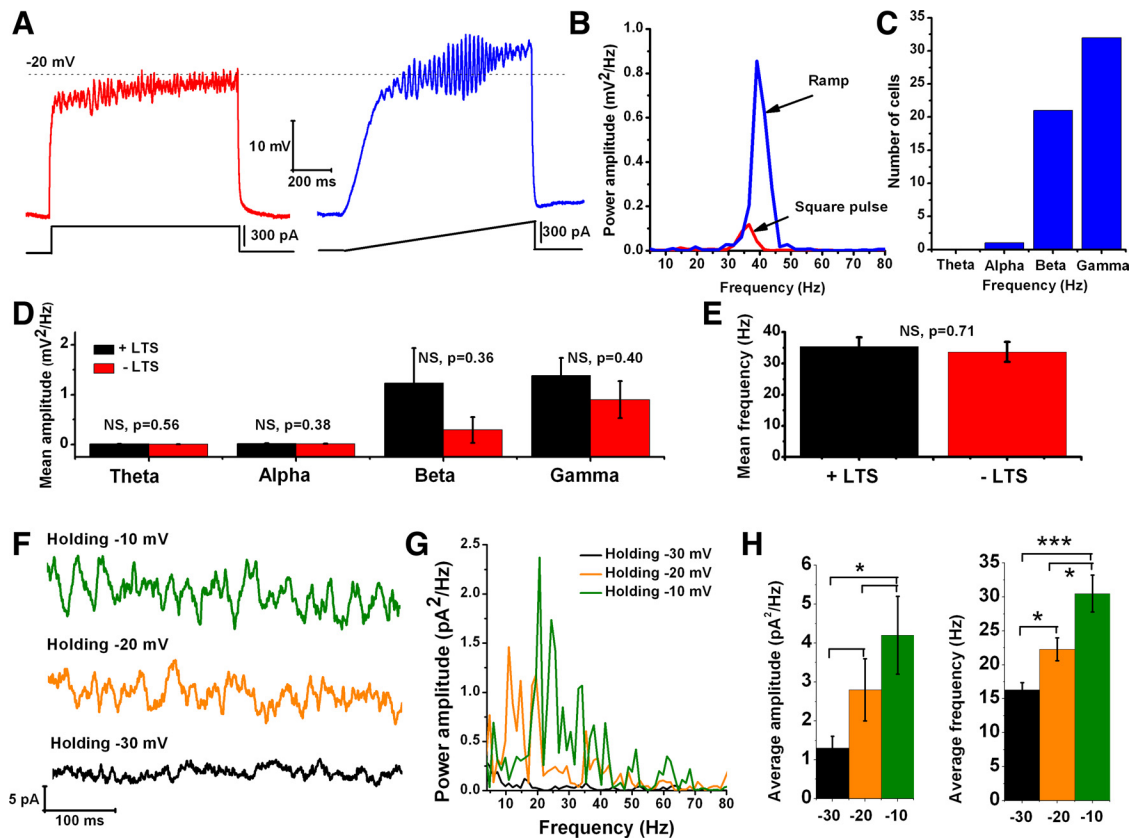
Fig. 3. All Pf neurons exhibited gamma band oscillations when depolarized. *A*: representative membrane potential responses of the same Pf neuron to depolarizing 1-s square steps (red record) and to 1-s-long ramps (blue record) obtained in the presence of fast synaptic blockers and TTX. *B*: overlapping curves comparing power spectrum amplitudes for oscillations obtained in *A*, pulses vs. ramps. Note the higher amplitude of the oscillations obtained in the same neuron using ramps vs. square steps. The membrane potential of this cell was -55 mV. *C*: histogram of the aggregate data showing the distribution of highest oscillatory peaks across the different frequency ranges for all the control neurons in this study ($n = 53$). *D*: bar graph showing the mean amplitudes of oscillations obtained during 1-s ramps for cells with ($+$LTS; black bars, $n = 35$) and without LTS ($-$LTS; red bars, $n = 18$) across all frequencies (theta, 3–7 Hz; alpha, 8–11 Hz; beta, 12–29 Hz; and gamma, 30–90 Hz). Note that the presence of LTS currents did not affect the amplitude of the oscillations at any frequency. *E*: bar graph showing the mean frequency of the oscillations in cells with (black bar) and without LTS (red bar). Note that the presence or absence of LTS currents did not affect the frequency of the oscillations. NS, no significant difference. *F*: representative current records obtained from a Pf neuron (10 days old) voltage-clamped to holding potentials of -30 (black record), -20 (orange record), and -10 mV (green record). *G*: power spectra corresponding to the current records shown in *F*. Note the increase in power of beta/gamma band frequency (20–90 Hz, green record) at -10 mV and mostly lower frequencies (10–19 Hz) at -20 mV in this 10-day-old cell. Both current- and voltage-clamp recordings were performed by combining high-K$^+$ intracellular solution and fast synaptic blockers and TTX. *H*: graph showing the average amplitude of the oscillations for the 9- to 12-day age group during different holding potentials (*left*). Graph at *right* shows the average frequency at different holding potentials for the same age group. *$P < 0.05$; **$P < 0.01$; ***$P < 0.001$.

ramps in the same cell (Fig. 3, *A* and *B*, blue records). Therefore, we continued using current ramps to characterize the oscillatory properties of Pf cells in the rest of the experiments. Statistical analysis showed that the power spectrum amplitude of the oscillations generated by the ramps was significantly higher than that generated by the current steps ($n = 42$, df $= 97$, $t = 7.6$, $P < 0.001$) (Fig. 3*B*). Oscillations were visible between the -20- and -5-mV somatic membrane voltage range and were absent at membrane potentials below -20 mV or above 0 mV. Power spectrum analysis of the membrane oscillations induced during ramp recordings revealed that 60% of the cells (32 of 53) exhibited the highest peak of oscillatory activity at the gamma range (30–60 Hz), whereas some (38%, or 21 of 53) cells had the highest peak at beta (12–29 Hz, $n = 20$) or alpha (8–11 Hz, $n = 1$) frequency ranges (Fig. 3*C*). However, those cells showing frequencies below gamma band were typically at early ages (see below).

In another group of cells tested, we found that 66% ($n = 35$) of the cells recorded had LTS currents and 34% ($n = 18$) did not. Interestingly, further analysis of their oscillatory properties

revealed that LTS currents had no effect on the amplitude of the oscillations at any frequency range, from theta ($P = 0.56$) through gamma ($P = 0.40$) (Fig. 3*D*). Furthermore, statistical analysis of the average oscillatory frequency (Fig. 3*E*) showed no significant difference ($P = 0.71$) between cells with LTS (35.5 ± 2.9 Hz) and cells without LTS (33.7 ± 3.2 Hz). These data suggest that T-type calcium channels do not play a significant role in the manifestation of the high-threshold oscillatory activity of Pf neurons.

Using voltage-clamp mode, we determined whether gamma band oscillations could be observed when the holding potential was varied from -30 to -10 mV (using 1-s-long depolarizing steps). Moreover, with voltage clamp, more positive membrane potentials were reached using steps, thus surpassing the -20-mV limit observed in our current-clamp recordings (see e.g., the response to a square step shown in Fig. 3*A*). In our initial experiments, the holding potential was set at -50 mV (close to the observed Pf neuron average resting membrane potential), and voltage steps were applied to reach holding potentials ranging from -50 to 0 mV. No clear oscillatory

currents were observed at holding potentials below −30 mV (Fig. 3F, black record). However, clear oscillations at alpha and beta ranges were observed in the power spectra at both −20- and −10-mV holding potentials and at gamma range at −10-mV holding potentials (Fig. 3F, orange and green records, respectively). Power spectra showed voltage dependence for a broad range of frequencies including alpha, beta, and gamma band frequencies (Fig. 3G). The highest gamma band power amplitudes were observed at a −10-mV holding potential (n = 29). The power spectrum analysis for 9- to 12-day-old cells showed that the average amplitudes of the oscillations at −10 mV were significantly higher than at −30 mV (P = 0.02; t = −2.7; df = 13; n = 14) (Fig. 3H, left). Interestingly, the amplitudes of the oscillations at −10, −20, and −30 mV were not statistically different across the three age groups (9–12 vs. 13–16 vs. 17–25 days; data not shown). These results revealed that the amplitude of the oscillations in voltage clamp was not age dependent. Furthermore, we analyzed the change in frequency at different holding potentials (Fig. 3H, right). The frequency increased with higher depolarizing levels in the 9- to 12-day age group (−10 vs. −20 mV, P = 0.03; −10 vs. −30, P < 0.001; −20 vs. −30, P = 0.01) (Fig. 3H, right). A similar relationship between the three holding potentials was observed in the other two age groups (data not shown). However, unlike amplitude, the frequency of the oscillations was age dependent. At the −10-mV holding potential, the age group at 17–25 days (73 ± 7 Hz) had a higher average frequency of oscillations compared with age groups at 9–12 (31 ± 3 Hz) and 13- 16 days (39 ± 6 Hz) (P < 0.001 and P = 0.01, respectively). That is, the average frequency of the oscillations increased by 26% between 9–12 and 13–16 days, whereas the total increase in average frequency from animals at 9–12 to 17–25 days of age was 135%. At the −20-mV holding potential, the age group at 17–25 days (47 ± 4.3) had a higher average frequency of oscillations compared with the age groups at 9–12 (22 ± 2 Hz) and 13–16 days (23 ± 4 Hz) (P < 0.001 and P = 0.003, respectively). Therefore, the average frequency of the oscillations increased by 5% between 9–12 and 13–16 days, whereas the total increase in average frequency from animals at 9–12 to 17–25 days of age was 114%. Finally, at the −30-mV holding potential, the age group at 17–25 days (36 ± 4 Hz) had a higher average frequency of oscillations compared with the age groups at 9–12 (16 ± 1 Hz) and 13–16 days (16 ± 2 Hz) (P < 0.001 and P = 0.002, respectively). The average frequency of the oscillations at this holding potential did not increase from 9–12 to 13–16 days, whereas the total increase in average frequency from animals at 9–12 to 17–25 days of age was 125%. The amplitudes of the peaks in the power spectrum were reduced after series resistance compensation (40–60%; i.e., to reduce any space clamp problems), suggesting that Pf neuronal oscillatory activity in voltage clamp was generated in neuronal compartments distant from the soma, as previously shown for "specific" thalamic relay neurons (Pedroarena and Llinas 1997). That is, somatic voltage-clamp ramps allowed distal calcium and/or potassium channels to open and, therefore, were able to modulate gamma band activity recorded by the somatic pipette.

Effects of carbachol on Pf neuronal oscillations. In our previous study on postsynaptic responses of Pf neurons exposed to CAR, we observed that 93% of Pf neurons responded to CAR (Ye et al. 2009). In the present study, we wanted to determine whether CAR (30 μM) superfusion had an effect on the frequency of the ramp-induced oscillations in single Pf neurons. We used 1-s ramp protocols, as described above, and the same extracellular solution containing fast synaptic blockers and TTX. CAR was continuously circulated in the bath solution. We recorded a group of 34 neurons of different age groups and compared their responses to those of cells recorded without CAR. Our results showed that cells exposed to CAR manifested higher frequencies of ramp-induced oscillations. We divided the cells into three developmental groups (9–12, 13–16, and 17–25 days) that showed differences in the frequency of oscillations in response to CAR (Fig. 4). Representative recordings from the first group (9–12 days) are shown in Fig. 4, A and B (no CAR, blue record; with CAR, red record). In both cells, the highest amplitude oscillations were observed at approximately −20 mV. The power spectrum of these records shows that the frequency of oscillations in the presence of CAR (red, 42 Hz) was higher than the frequency of oscillations in the same age cell without CAR (blue, 27 Hz) (Fig. 4C). In addition, we analyzed the average oscillatory frequency of all recorded cells in this age group (9–12 days). The graph in Fig. 4D shows the distribution of oscillatory frequencies for all recorded cells without CAR (blue dots, n = 20) and with CAR (red dots, n = 17). Statistical analysis revealed that, during ramps, all cells exposed to CAR fired at significantly higher frequencies (41.7 ± 4.3 Hz) compared with control extracellular solution (24.6 ± 3.8 Hz) (1-way ANOVA, df = 36, t = 5.4, P < 0.001). The next age group (13–16 days) exhibited the same oscillatory characteristics as the previous group with the highest oscillatory amplitudes evident at approximately −20 mV (Fig. 4, E and F). CAR increased the oscillatory frequency of Pf neurons in this age group, as well (see the power spectrum in Fig. 4G). The graph in Fig. 4H shows the distribution of oscillatory frequencies of cells recorded without CAR (blue dots, n = 21) and with CAR (red dots, n = 11). The average oscillatory frequency for the cells recorded under CAR (55.2 ± 3 Hz) was significantly higher than those recorded without CAR (35.1 ± 2.9 Hz) (1-way ANOVA, df = 31, t = 4.4, P < 0.001). Finally, we analyzed the oscillatory frequencies of the oldest age group (17–25 days). Representative records of control cells (no CAR, blue record) and those recorded with CAR (red record) are shown in Fig. 4, I and J. The oscillatory frequency was 47 Hz (blue) for the control cell and 72 Hz (red) for the cell recorded in the presence of CAR (Fig. 4K). However, when we analyzed the oscillatory frequencies of all the cells in this age group, we found that there was no statistical difference between the CAR-treated (n = 6) and untreated cells (n = 12) (Fig. 4M) (1-way ANOVA, df = 17, t = 1.1, P = 0.31). Interestingly, CAR had no effect on the amplitudes of the oscillations at any age group (9–10 days: df = 36, t = 0.6, P = 0.55; 12–16 days: df = 31, t = −1.3, P = 0.19; 17–25 days: df = 17, t = 0.06, P = 0.95). Similarly to what we reported in our previous study on the oscillatory properties of PPN neurons (Kezunovic et al. 2011), CAR also significantly increased the input resistance of Pf neurons (1-way ANOVA, df = 83, t = 2.3, P = 0.02). In summary, our data showed that, early in the development of Pf neurons, their maximal oscillatory frequency begins at lower ranges (alpha and beta) and gradually plateaus at gamma range with age (Fig. 4N, blue line). However, CAR could increase the firing frequency of younger cells to the gamma range, but their

frequency would eventually plateau within the gamma range, but no higher (Fig. 4*N*, red line). In the oldest age group, CAR did not significantly increase frequency beyond the gamma range.

Effects of specific calcium channel blockers on Pf neuronal oscillatory activity. The range of membrane potentials at which gamma band oscillations were observed in the Pf nucleus overlapped with that of high-threshold voltage-dependent calcium channel activation voltages described in the cortex and thalamus (Caterall 1998; Hille 2001; Llinas 1988). Therefore, we studied the effects of both ω-Aga (a P/Q-type calcium channel blocker, 200 nM) and ω-CgTx (a N-type calcium channel blocker, 2.5 μM) on a total of 35 Pf neurons. The P/Q-type channel blocker ω-Aga totally abolished gamma band oscillations ($n = 7$). Figure 5*A* shows control (black), blockade

(gray; ω-Aga), and recovery (black; washout) records of oscillations in a representative neuron. Figure 5*B* shows the power spectrum of the oscillations during control (black), blockade (gray), and recovery (black). The effect of the toxin was reversed during washout (black record), which consisted of the same extracellular solution as in the control condition, including fast synaptic blockers and TTX. Moreover, bath preapplication (>30 min) of ω-Aga prevented Pf neurons from oscillating at higher frequencies ($n = 2$). Interestingly, the N-type blocker ω-CgTx only reduced gamma band oscillation amplitude, as evident in the power spectrum (Fig. 5, *C* and *D*; $n = 8$; gray record). The ω-CgTx effect was also reversed during washout (black record), and the amplitude of gamma band oscillations returned to almost the same level as in the control. Bath preapplication of ω-CgTx did not prevent Pf neurons
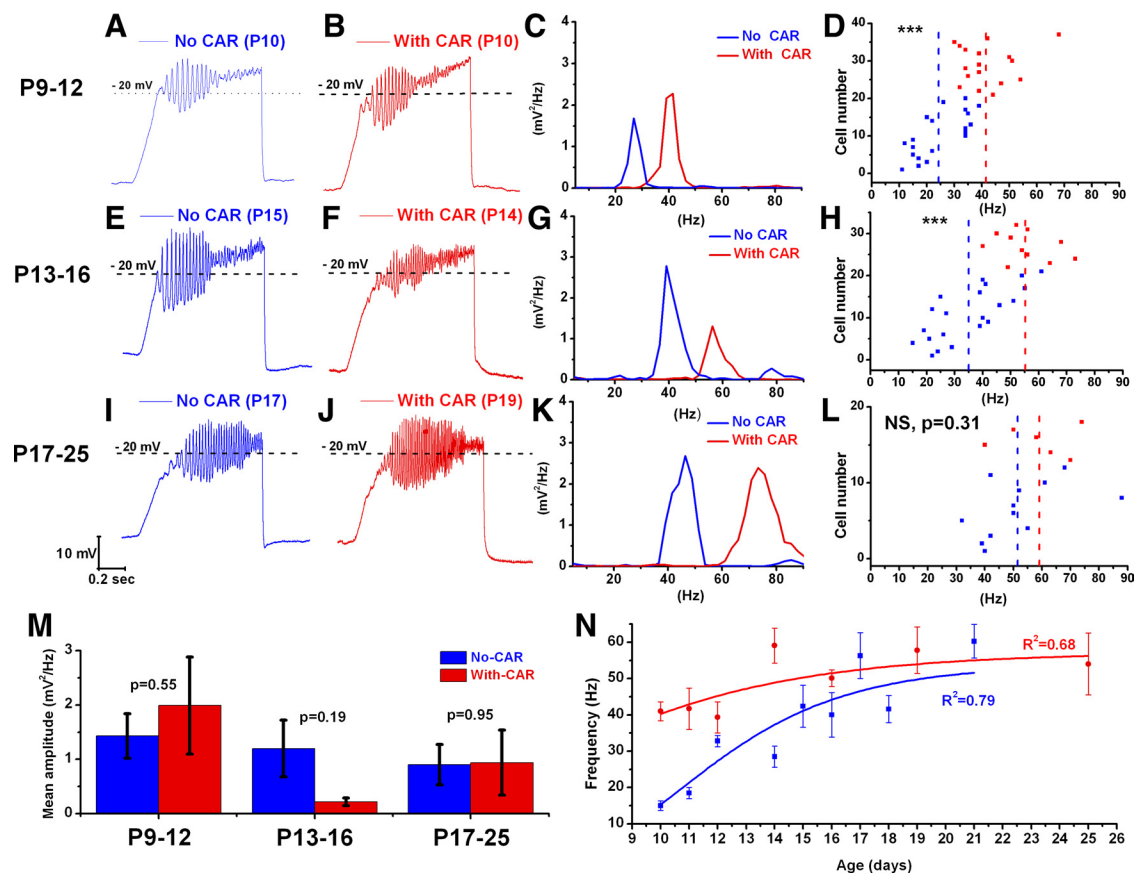

Fig. 4. Carbachol (CAR) increased the frequency of membrane potential oscillations in Pf neurons. *A* and *B*: representative membrane potential oscillations of a (10 day old) Pf neuron in the presence of CAR (red record) and without CAR (blue record) in the extracellular solution, obtained during 1-s-long ramps. *C*: power spectrum of the records in *A* and *B*. *D*: graph showing the maximal firing frequency of each individual cell in the 9- to 12-day age range (P9–12). Blue dots represent cells recorded in the control condition (no CAR; $n = 20$), and red dots denote cells recorded in the presence of CAR ($n = 17$). The average firing frequency of the cells recorded with CAR (red dashed line) was significantly higher than in those without CAR (blue dashed line). ***$P < 0.001$. *E* and *F*: representative membrane potential oscillations of Pf neurons in the presence of CAR (red record, P14) and without CAR (blue record, P15) recorded under the same conditions as in *A* and *B*. *G*: power spectrum of the records in *E* and *F*. *H*: graph showing the maximal firing frequency of each individual cell at P13–16. Blue dots represent cells recorded in the control condition (no CAR; $n = 21$), and red dots cells recorded in the presence of CAR ($n = 11$). The average firing frequency of the cells recorded under CAR (red dashed line) was significantly higher than in those without CAR (blue dashed line). ***$P < 0.001$. *I* and *J*: representative membrane potential oscillations of Pf neurons in the presence of CAR (red record, P19) and without CAR (blue record, P17) recorded under the same conditions as in *A* and *B*. *K*: power spectrum of the records in *I* and *J*. *L*: graph showing the maximal firing frequency of each individual cell in at P17–25. Blue dots represent cells recorded in the control condition (no CAR; $n = 12$), and red dots cells recorded in the presence of CAR ($n = 6$). At this age range, there was no statistical difference ($P = 0.31$) in maximal firing frequency of cells recorded in the presence of CAR (red dashed line) vs. cells in control conditions (blue dashed line). *M*: bar graph showing the mean amplitude of membrane potential oscillations for the cells recorded without (blue bars) and with CAR (red bars) across the 3 age groups. Note that CAR did not affect the amplitude of the oscillations at any age. *N*: graph showing the distribution of mean firing frequencies of Pf neurons recorded without (blue squares) and with CAR (red squares) in the extracellular solution during the developmental period used in this study (9–25 days). Blue (no CAR) and red (with CAR) lines represent the best-fit lines of the corresponding data. Note that the lines almost merge later in development. All experiments were conducted in the presence of fast synaptic blockers and TTX.
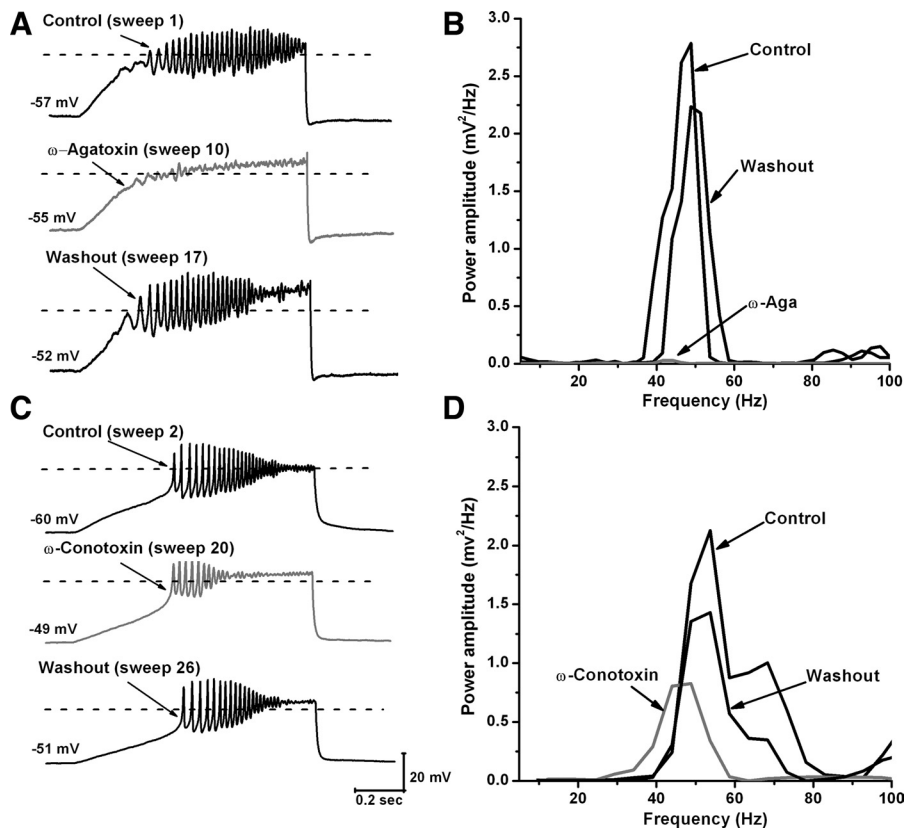
Fig. 5. N- and P/Q-type calcium channels mediate the depolarizing phase of gamma band oscillations in the Pf nucleus. *A*: representative membrane potential oscillations obtained during 1-s-long ramps before specific calcium channel blocker application (control; black record), after bath application of ω-agatoxin-IVA (ω-Aga; 200 nM; gray record), and after washout (black record). Note the elimination of oscillations by the P/Q-type channel blocker ω-Aga and the return of the oscillatory activity after only 7 min of washout. *B*: power spectrum of the records shown in *A*. *C*: representative membrane potential oscillations obtained during 1-s-long ramps before specific calcium channel blocker application (black record), after bath application of ω-conotoxin-GVIA (ω-CgTx; 2.5 μM; gray record), and after washout (black record). Note the reduction of the amplitude of the oscillations after application of the N-type calcium channel blocker ω-CgTx and the return of the oscillatory amplitude after washout after only 6 min. *D*: power spectrum of the records shown in *C*. All cells were recorded in the presence of fast synaptic blockers and TTX. Dashed lines in *A* and *C* represent the -20-mV membrane potential.

from oscillating. However, the amplitude of those oscillations was significantly lower than in control conditions ($n = 12$) (1-way ANOVA, df $= 58$, $t = -2.2$, $P = 0.03$). These results showed that both voltage-dependent P/Q- and N-type calcium channels may mediate the depolarizing phase of gamma band oscillations in the Pf nucleus. However, only P/Q-type channels appeared to be essential for gamma band oscillation generation. The specific calcium channel blockers had the same type of blocking effect on Pf neuron oscillatory activity regardless of age. Furthermore, ω-Aga blocked the CAR-enhanced ramp-induced oscillations ($n = 5$). This finding strengthens the argument that P/Q-type calcium channels play a crucial role in the oscillatory behavior of Pf neurons.

Characterization of high-threshold calcium channel types present in Pf neurons. To evaluate the subtypes of high-threshold calcium currents present in Pf neurons, depolarizing voltage square pulses were employed in combination with high-Cs$^+$/QX-314 in the intracellular pipette solution and bath-applied fast synaptic receptor blockers (see METHODS) using slices from three developmental age groups: 9–12, 13–16, and 17–25 days. We pursued the characterization of high-threshold calcium channel types in a total of 124 Pf neurons, studying the currents mediated by P/Q- and N-type calcium channels in these neurons. We recorded calcium currents 2–4 min after gaining access to the neuronal intracellular compartment, to allow proper delivery of intracellular solution into all neuronal compartments, thus decreasing space clamp problems. Recording of calcium currents lasted for more than 30 min without significant rundown. The holding potential was initially clamped at -70 mV and then depolarized up to 20 mV, using 150-ms square voltage steps. Clear T-type calcium currents were observed in 74% of Pf neurons studied in all three age

groups. T-type calcium currents were manifested as a depolarizing membrane shift during 150-ms square pulses from -70 to -40 mV (Fig. 6*A*, *left*, black line), whereas they were totally inactivated at holding potentials of -50 mV and higher (Fig. 6*A*, *left*, red line). On the other hand, high-threshold currents peaked at -10 mV and showed a typical long-lasting current when Pf cells were depolarized from holding potentials of -70 mV (Fig. 6*A*, *right*, black line), presenting only a slight inactivation at holding potentials of -50 mV (Fig. 6*A*, *right*, red line). High-threshold currents were abolished by the simultaneous application of ω-Aga (200 nM) and ω-CgTx (2.5 μM), leaving the T-type currents unaffected (Fig. 6*B*). These results confirmed that both P/Q- and N-type were mediating high-threshold calcium currents in Pf neurons in all age groups. P/Q- and N-type, but not T-type, channels were clearly activated at holding potentials above -50 mV, confirming that high- but not low-threshold calcium channels mediate gamma band oscillatory activity of Pf cells when depolarized above -50 mV.

Current-voltage (*I–V*) curves were obtained for both T-type and high-threshold current components. We plotted current density values (pA/pF) against voltage measured at the beginning and at the end of square steps (Fig. 6*B*, *right*, open and filled circles, respectively). Figure 6*C* shows the *I–V* curve of calcium currents recorded from Pf cells at 9–12 days. T-type mediated currents peaked at a holding potential of -40 mV, whereas high-threshold P/Q- and N-type mediated currents presented maximum values at a holding potential of -10 mV. Average current density values for the three age ranges were significantly different (Table 2). Calcium current densities at -40 and -10 mV from Pf cells at 13–16 days were similar to those recorded at 17–25 days, which allowed us to pool these age groups into a new 13- to 25-day group (Table 2).
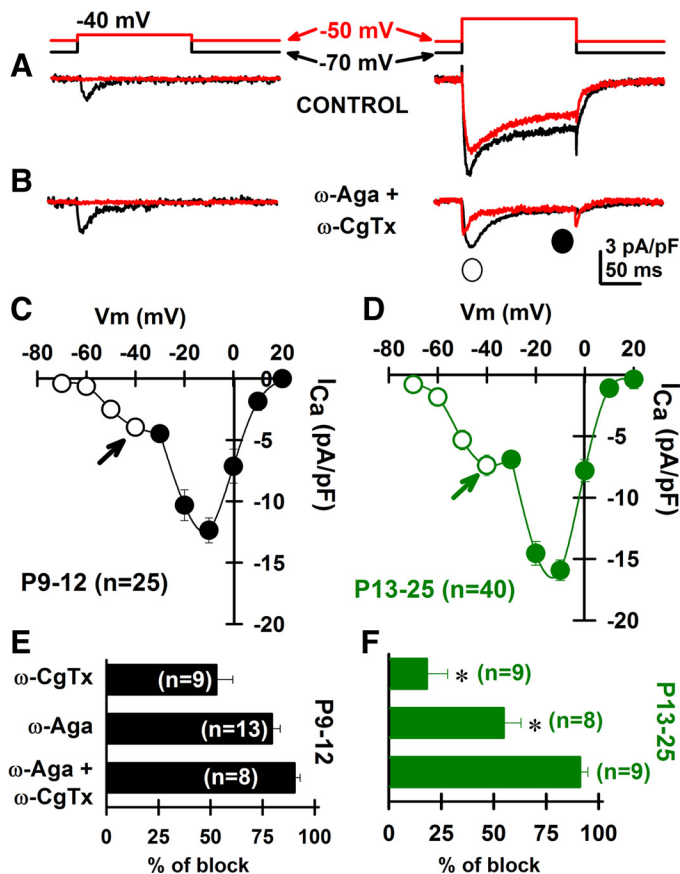
Fig. 6. Both N-type and P/Q-type calcium channels are present in Pf neurons. *A*: representative calcium currents obtained using depolarizing square steps to either −40 (*left*) or −10 mV (*right*) from both −70-mV (black lines) and −50-mV (red lines) holding potentials. Note that T-type calcium currents were inactivated at the −50-mV holding potential. *B*: same as in *A*, after bath application of ω-CgTx (2.5 μM) + ω-Aga (200 nM). *C* and *D*: average current density-voltage (*I–V*) curve for Pf cells from P9–12 (*n* = 25) and P13–25 (*n* = 40) age groups, respectively. Note the presence of higher T-type peak current densities for Pf neurons from older animals (P13–25; green arrow in *D*) compared with younger animals (P9–12; black arrow in *C*). *E* and *F*: average percentage of blocked calcium current amplitude after ω-CgTx (2.5 μM), ω-Aga (200 nM), and ω-CgTx + ω-Aga for Pf neurons from either P9–12 (*E*) or P13–25 (*F*) age groups, respectively. *P < 0.05.

Interestingly, the peak (holding potential −40 mV) T-type current density values were significantly increased after postnatal *day 12*, without affecting the peak density of P/Q- and N-type currents (Table 2). Indeed, average *I–V* values from 13- to 25-day-old Pf cells showed an increase in T-type current density without changing high-threshold current density (Fig. 6*D*).

Table 3 summarizes the results obtained across the three age groups for the frequency of AP firing during current steps compared with the frequency of ramp-induced oscillations and

ramp-induced oscillations following CAR exposure. Briefly, the frequency of AP firing in Pf cells at the beginning of the current steps was 46–55 Hz (gamma) but decreased to 23–24 Hz (beta) during the remainder of the step. Taking these data together, the mean frequency of firing induced by steps across the entire step was 31–36 Hz (gamma). These data show that the only significant change over age was the initial AP frequency (46 vs. 55 Hz). The application of ramps resulted in a mean frequency of oscillations of 24–51 Hz, which significantly increased with age (from beta to gamma). The effects of CAR on ramp-induced oscillations resulted in frequencies of 41–59 Hz (gamma). These data showed that CAR increased the frequency of ramp-induced oscillations at the two earlier ages but not in the oldest animals, since the ramp-induced oscillation frequency in older animals had plateaued and CAR was unable to drive the frequency above 60 Hz.

To determine the proportion of P/Q- and N-type calcium channels mediating calcium currents in Pf neurons, we bath-applied the specific calcium channel blockers ω-Aga (200 nM) and/or ω-CgTx (2.5 μM) (both individually and combined) during calcium current recordings using −10-mV square steps. A maximal effect of the toxins was usually achieved after 15 min of continuous superfusion. Both ω-CgTx and ω-Aga reduced high-threshold calcium currents in Pf neurons at 9–12 (Fig. 6*E*, black) and 13–25 days (Fig. 6*F*, green). The combination ω-CgTx + ω-Aga abolished calcium currents in all cells of both age groups (Fig. 6, *E* and *F*). Importantly, a lower percentage induced calcium current was observed in Pf neurons at 9–12 days compared with 13–25 days when using ω-CgTx (Fig. 6, *E* and *F*; Student's *t*-test, *n* = 18, df = 7, *t* = 2.8, *P* = 0.03) and when using ω-Aga (Fig. 6, *E* and *F*; Student's *t*-test, *n* = 21, df = 10, *t* = 2.7, *P* = 0.02). The combination of ω-CgTx + ω-Aga had a similar blocking effect in both age groups (Fig. 6, *E* and *F*; Student's *t*-test, *n* = 17, df = 14, *t* = 0.2, *P* = 0.88). In conclusion, our results suggest a dual contribution of both high-threshold P/Q- and N-type calcium channels to the total calcium currents in Pf cells at depolarized membrane potentials.

DISCUSSION

In the present study, we found that Pf neurons fired at gamma band frequency, but no higher, when maximally activated, and manifested the intrinsic membrane properties that allow them to oscillate at these frequencies. These oscillations appeared to be calcium channel dependent and plateaued at higher frequencies within the gamma band range later in development, and ramp-induced oscillations at these frequencies could be increased by the nonspecific cholinergic agonist CAR, but only at earlier ages. That is, CAR did not increase the already plateaued maximal firing frequency above gamma

Table 2. *Calcium current density of Pf neurons recorded during different ages*

	P9–12	P13–16	P17–25	P13–25
n	25	22	18	40
I_{Ca} density (holding −40 mV), pA/pF	−3.96 ± 0.37	−8.48 ± 1.43*	−7.03 ± 0.46	−7.84 ± 0.88*
I_{Ca} density (holding −10 mV), pA/pF	−12.4 ± 1.02	−16.4 ± 1.3	−13.4 ± 0.82	−14.9 ± 0.8

Values are means ± SE. *P < 0.05 compared with P9–12 densities (1-way ANOVA, Bonferroni post hoc test; holding −40 mV: P9–12 vs. P13–16: df = 20, *t* = 3.5, *P* < 0.05; P9–12 vs. P17–25: df = 20, *t* = 2.2, *P* > 0.05; P13–16 vs. P17–25: df = 16, *t* = 0.7, *P* > 0.05; P9–12 vs. P13–25: df = 23, *t* = 3.3, *P* < 0.05; holding −10 mV: all comparisons with P9–12 group were not significant). I_{Ca}, calcium current.

Table 3. *Frequency of induced AP during steps and membrane oscillations during ramps with and without CAR*

Age Group	Mean AP Frequency During Steps			Mean Oscillation Frequency During Ramps	
	1st ISI	Steady state (middle + last + ISI)	Overall	TTX + blockers	TTX + blockers + CAR
P9–12	46.4 ± 3.7	23.4 ± 0.8	31.1 ± 2.2	24.6 ± 3.8	41.7 ± 4.3
P13–16	45.4 ± 3.9	22.4 ± 1.2	30.1 ± 2.3	35.1 ± 2.9	55.2 ± 3.1
P17–25	55.4 ± 4.7	24.1 ± 1.4	36.5 ± 4.1	51.6 ± 4.1	59.2 ± 4.7

Values are means ± SE of frequency (in Hz) of induced action potentials (AP) during steps and of membrane oscillations during ramps and after exposure to carbachol (CAR). AP data were calculated from the 180-pA calcium current depolarization step (i.e., last step). Oscillation data were composed from analysis of peaks in the power spectra in the presence of fast synaptic blockers and tetrodotoxin (TTX). ISI, interspike interval.

band in the oldest cells studied, suggesting that CAR may accelerate the manifestation of higher gamma band oscillatory activity by Pf cells during development. Moreover, the mechanism behind the generation of these oscillations appears to involve high-threshold voltage-dependent P/Q- and N-type calcium channels. This is the first time such physiological characteristics have been described in Pf neurons. The significance of these findings is amplified in light of recent discoveries of similar oscillatory mechanisms in the PPN and the dorsal subcoeruleus (SubCD) nuclei, both part of the reticular activating system (RAS). There is now little doubt that a number of nuclei in the RAS have the ability to manifest gamma band activity, similar to that reported in cortical, hippocampal, thalamic, and cerebellar cells.

In the striatum, subthalamic nucleus, and prefrontal cortex, depolarizing current steps linearly increase the firing frequency of APs up to 100 Hz or higher (Azouz et al. 1997; Barraza et al. 2009; Povysheva et al. 2008). On the other hand, pyramidal cells in mouse neocortex plateau below gamma band frequency, even after application of very high amplitude current steps (600–1,000 pA) (Zhou et al. 2010). In this study, we showed that when Pf neurons are depolarized using increasing amplitude current steps, they fired initially at higher frequency within the gamma band, but the firing frequency slowed and plateaued in the beta range (Fig. 2B). However, the average firing frequency for the entire step plateaued in the gamma range (~35 Hz). This plateau in firing rate was observed in all Pf cells. Similar results have been observed in the PPN and the SubCD nuclei (Simon et al. 2010, 2011). The present results demonstrate that all Pf neurons exhibited gamma band AP frequency when maximally activated, as well as gamma band membrane oscillations. This newly discovered property of Pf neurons may represent a novel mechanism for the induction of activated states, such as waking, by Pf efferents.

Our five-step pyramidal experiments (Fig. 2C) showed that oscillatory activity replaced AP firing during high-amplitude depolarizing steps, similar to that observed in PPN neurons (Simon et al. 2010), thus suggesting that the mechanism behind similar plateau frequencies observed is related to the fact that gamma oscillations can drive AP generation by depolarizing membrane potential toward AP threshold, as previously described for "specific" thalamic neurons (Pedroarena and Llinas 1997). The fact that the membrane potential of Pf cells could oscillate at the gamma band range when P/Q-type channels were blocked suggests that N-type channels might act as an additional "security factor" to reliably generate AP discharge at such a high frequency range. Current steps, however, were unable to drive the membrane potential to sufficiently depolarized levels, probably due to the activation of potassium

channels (above −20 mV from a holding potential of −50 mV). Moreover, recent studies have shown high-amplitude afterhyperpolarization in different thalamic neurons (Zhang et al. 2009). This potential property, as well as the activation of potassium channels, may have prevented square steps from reaching a membrane potential at which high-threshold oscillations could be observed. Additional current was needed to reach such membrane potential levels such as those attained when using ramps, as previously reported for PPN neurons (Kezunovic et al. 2011). In the natural condition, depolarization, probably mediated by sodium channel-dependent APs, appears to be responsible for spreading the membrane depolarization needed to open high-threshold calcium channels. Consequently, under our experimental conditions, it can be expected that, with the use of ramps, neurons voltage-clamped above −20 mV might show oscillatory activity. Our results indeed show that the membrane potential has to reach approximately −20 mV at the cell body and above for the high-threshold P/Q-type channels to open. Since we had to voltage clamp Pf neurons above −20 mV (above expected) to observe the oscillations, we suggest that these oscillations may occur in distal neuronal compartments such as the dendrites. This would be similar to the oscillations observed in "specific" TC relay neurons, which were visualized in the dendrites using calcium imaging (Pedroarena and Llinas 1997). Although it is impossible to determine the actual membrane potential of the dendrites without actually clamping them (voltage clamp of small dendrites would lead to rapid dialysis of the intracellular domain), their membrane potentials are possibly much lower than the −20-mV threshold induced at the soma, due to the accumulated membrane capacitance between the electrode and these dendritic compartments. Indeed, such levels of change in power were partially reduced after series resistance compensation. Therefore, the real threshold for these oscillations is probably much lower and closer to physiological values. Importantly, voltage-clamp experiments showed that calcium currents mediated by both P/Q- and N-type channels peaked at a holding potential of −10 mV (Fig. 3), consistently with the range of membrane potentials in which gamma band oscillations were evident (Fig. 4).

In "specific" TC neurons, LTS currents are part of their stereotypical intrinsic properties and are mediated by T-type calcium channels (Llinas and Steriade 2006). These calcium channels open in response to low-amplitude depolarization of the plasma membrane. The entry of two positive charges with every calcium ion leads to further depolarization of the membrane, the LTS, and opening of channels that have a higher threshold (Nelson et al. 2006). Llinas and Steriade (2006) consider this mechanism essential to inducing cortical synchro-

nization of high-frequency rhythms during waking and REM sleep (tonic pattern) and synchronization of low-frequency rhythms during SWS (LTS + I_h oscillations). Our data indicate that T-type calcium channels do not modulate the amplitude or frequency of ramp-induced high-threshold oscillations in Pf neurons. However, due to their preferential expression and their important pacemaker role in gating sodium and calcium channels (Nelson et al. 2006), T-type calcium channels probably help neurons reach highly depolarized levels, allowing high-threshold calcium channels to open. Here we showed an increase in T-type mediated current density in parallel with an increment in gamma band power during Pf development. Previous studies by ourselves (Phelan et al. 2005) and others (Beatty et al. 2009) showed that spindle-shaped Pf neurons recorded immediately adjacent to the fasciculus retroflexus exhibited low incidence (~20%) of T-type currents compared with "specific" thalamic neurons (Llinas and Steriade 2006). In the present study of calcium currents, we found a much higher incidence (66%) of these currents, suggesting that the threshold for eliciting these currents may be higher than usual, preventing their manifestation using simple hyperpolarizing steps as in previous studies.

Our data show that oscillatory activity plateaued in the gamma band range in older animals (17–25 days), which is also the period when the largest developmental decrease in REM sleep starts to level off at the adult REM sleep levels (Jouvet-Mounier et al. 1970). This is likely the period when high-threshold calcium channels are expressed sufficiently to enable Pf neurons to oscillate at high frequencies. Moreover, we showed that CAR could significantly increase the frequency of the ramp-induced oscillations of younger neurons, whereas it did not affect the presumably already capped frequency of older neurons. These results suggest that younger cells may need higher CAR-induced membrane potential depolarization to reach high-frequency gamma oscillations readily observed in older cell groups. In this sense, resting membrane potential and calcium current density increased during development (see Tables 1 and 2, respectively). Thus CAR may still induce depolarization toward high-threshold calcium channel opening in older Pf cells, but its subtle effects might be not be quantifiable using strong depolarizing current ramps. Muscarinic and nicotinic cholinergic receptors are involved in higher cognitive functions including synaptic plasticity and memory processes known to involve higher frequency oscillations in the gamma range (Von der Kammer et al. 2001). In the rat frontal cortex, CAR can induce changes in different signaling pathways, activating phosphoinositide turnover, translocating protein kinase C, and stimulating nitric oxide synthase activity (Sterin-Borda et al. 2003). These results suggest that, at younger ages, rat Pf neurons may need substantial activation by cholinergic input to reach the gamma band range. It is possible that modulation of these signaling pathways induced by CAR may be responsible for the increase in average frequency of oscillatory activity we observed with age.

High-threshold voltage-gated calcium channels require high membrane potentials to be reached in order for them to allow calcium into the cell. P/Q-type calcium channels are present throughout the brain (Hillman et al. 1991; Uchitel et al. 1992). These channels are found on the dendrites of bushy "specific" TC cells where they support gamma band oscillations (Pedroarena and Llinas 1997). These authors were able to visual-

ize calcium transients in the distal dendrites upon somatic injection of depolarizing current (in current-clamp mode) and therefore demonstrated that the P/Q-type currents were probably in the dendritic tree of these cells. This accounts for the "high threshold" nature of the channels, since the soma needs to be depolarized to high levels that may not be considered physiological, but the membrane potential at the dendrites is probably within physiological range. Pedroarena and Llinas (1997) also used barium as a current carrier showing greater amplitude of subthreshold gamma band oscillations of the membrane potential. Since barium blocks delayed rectifier potassium channels, among others, these authors suggested the opening-closing transitions of P/Q-type calcium channels and potassium channels might account for the generation of gamma oscillations in TC relay neurons.

In our previous study, using the same methods, we conclusively demonstrated that P/Q-type calcium channels play a major role in the generation of the rising phase of gamma band oscillations in PPN neurons (Kezunovic et al. 2011). Here, we report that long, sparsely branching neurons of the Pf nucleus that receive cholinergic input from PPN neurons manifest P/Q-type channel-dependent gamma band oscillatory activity, using whole cell patch clamp (in both current- and voltage-clamp experiments). Moreover, we have shown that N-type calcium channels play a role in these oscillations, similar to the kind of membrane properties reported for PPN neurons (Kezunovic et al. 2011). From a biophysical point of view, opening of both calcium channels (mostly P/Q, but also N-type) and delayed rectifier potassium channels was required to reach membrane potential oscillatory activity in the gamma band range for both PPN (Kezunovic et al. 2011) and Pf neurons (this work). This suggests that, unlike "specific" TC relay neurons, the PPN and Pf might have a dynamic mechanism of interaction between the opening of calcium and potassium channels. Additional experiments are needed to determine the distribution of these high-threshold calcium channels and delayed rectifier-like potassium channels during the development of Pf neurons, and to determine their exact anatomical locations. However, clear evidence is provided in this study showing that both P/Q- and N-type calcium channels mediate high-threshold calcium currents in Pf neurons. Moreover, a higher proportion of P/Q-type channels (i.e., manifested as a higher percentage of current blockade by ω-Aga) vs. N-type channels, might also explain why gamma band oscillation power increased with age. Such a developmental switch from N- to P/Q-type channels has been previously described for other structures in the brain stem (Iwasaki and Takahashi 1998) and throughout the brain (Iwasaki et al. 2000). Thus our results strongly suggest that P/Q-type channels in "nonspecific" Pf neurons play a key role in gamma band generation during development, similar to "specific" thalamic relay neurons (Llinas et al. 2007).

The centromedian-parafascicular (CM/Pf) complex of the thalamus (in rodents mostly Pf) has recently become an area of interest for deep brain stimulation (DBS) for the treatment of movement disorders, including Parkinson's disease (PD) (Jouve et al. 2010). Neurodegeneration of this complex has been reported in PD patients (Henderson et al. 2000), whereas in animal models of PD, complex alterations of CM/Pf activity have been reported (Aymerich et al. 2006; Freyaldenhoven et al. 1997; Orieux et al. 2000; Parr-Brownlie et al. 2009).

Interestingly, high-frequency stimulation (HFS) of the Pf nucleus in rodents showed moderate to strong antiparkinsonian benefits by recruiting basal ganglia circuitry (Jouve et al. 2010). CM/Pf complex HFS also counteracts dopamine lesion-induced akinetic deficits and overactivity of striatopallidal neurons (Kerkerian-Le Goff et al. 2008). In this study, we showed, at the single cell level, oscillatory gamma band activity in Pf neurons when maximally activated. We identified specific calcium channels that play a significant role in the generation of these oscillations. Since Pf neurons send widespread projections throughout the brain, the importance of this oscillatory activity may be considerable. It is possible that, instead of electrical stimulation of the CM/Pf complex, novel pharmacological treatments could be developed to target the oscillatory output of the Pf nucleus for the treatment of certain movement disorders.

Because gamma waves can occur during slow wave states and anesthesia, a close relation to consciousness has been questioned (Vanderwolf 2000). Recent studies in humans have confirmed animal studies showing that gamma oscillations are transiently expressed during up states during SWS, representing patterns that restore "microwake" activity and may be related to memory processes (Le Van Quyen et al. 2010). It has been suggested that consciousness is associated with continuous gamma band activity, as opposed to an interrupted pattern of activity (Vanderwolf 2000). The original description of the RAS specifically suggested that it participates in "tonic" or continuous arousal (Moruzzi and Magoun 1949), and lesions of this region were found to eliminate tonic arousal (Watson et al. 1974). It is possible that PPN input to the Pf helps maintain such activity. This raises the question of how a circuit can maintain such rapid, recurrent activation for prolonged periods. Expecting a circuit of 6 or 10 synapses to reliably relay 40- to 60- or even 90-Hz cycling without failing is unrealistic. Without the intrinsic properties afforded by rapidly oscillating channels, such as those described recently for PPN, Pf, and subthreshold oscillations in SubCD, beta/gamma band activity could not be maintained. The combination of channels capable of fast oscillations and circuitry that involves activating these channels probably are both required for the maintenance of gamma band activity (Kezunovic et al. 2011; Llinas 1988; Llinas et al. 1991, 2002, 2007). The group of nuclei named, in which every cell in every nucleus exhibits beta/gamma band activity, may have a role in maintaining overall beta/gamma activity. We speculate that it is the continued activation of the RAS during waking that allows the maintenance of the background of gamma activity necessary to support a state capable of reliably assessing the world around us on a continuous basis.

The present findings provide novel insights into the function of the Pf, demonstrating that this element of the RAS generates gamma band oscillatory activity in the presence of sufficient excitation. We suggest that, rather than participating in the temporal binding of sensory events, gamma band activity generated in the Pf may help stabilize coherence related to arousal, providing a stable activation state during waking, and relay such activation to the cortex, which thus participates in "nonspecific" thalamocortical processing. Much work is needed to support this speculation, but the intriguing findings described here certainly provide a starting point for such investigations. These results may have implications for studies of arousal and anesthesia, suggesting that this subcortical region preferentially fires at gamma band frequencies and may be directly modulated by stimulants and anesthetics.

DISCLOSURES

No commercial support or off-label/investigational use is declared by the author(s).

REFERENCES

Aymerich MS, Barroso-Chinea P, Pérez-Manso M, Muñoz-Patiño AM, Moreno-Igoa M, Gonza'lez-Herna'ndez T, Lanciego JL. Consequences of unilateral nigrostriatal denervation on the thalamostriatalpathway in rats. *Eur J Neurosci* 23: 2099–2108, 2006.

Azouz R, Gray CM, Nowak LG, McCormick DA. Physiological properties of inhibitory interneurons in cat striate cortex. *Cereb Cortex* 7: 534–545, 1997.

Barraza D, Kita H, Wilson CJ. Slow spike frequency adaptation in neurons of the rat subthalamic nucleus. *J Neurophysiol* 102: 3689–3697, 2009.

Beatty JA, Sylwestra EL, Cox CL. Two distinct populations of projection neurons in the rat lateral parafascicular thalamic nucleus and their cholinergic responsiveness. *Neuroscience* 162: 155–173, 2009.

Capozzo A, Florio T, Cellini R, Moriconi U, Scarnati E. The pedunculopontine nucleus projection to the parafascicular nucleus of the thalamus: an electrophysiological investigation in the rat. *J Neural Transm* 110: 733–747, 2003.

Caterall WA. Structure and function of neuronal Ca^{2+} channels and their role in neurotransmitter release. *Cell Calcium* 24: 307–323, 1998.

Erro E, Lanciego JL, Gimenez-Amaya JM. Relationships between thalamostriatal neurons and pedunculopontine projections to the thalamus: a neuroanatomical tract-tracing study in the rat. *Exp Brain Res* 127: 162–170, 1999.

Freyaldenhoven TE, Ali SF, Schmued LC. Systemic administration of MPTP induces thalamic neuronal degeneration in mice. *Brain Res* 759: 9–17, 1997.

Garcia-Rill E, Charlesworth A, Heister D, Ye M, Hayar A. The developmental decrease in REM sleep: the role of transmitters and electrical coupling. *Sleep* 31: 673–690, 2008.

Henderson JM, Carpenter K, Cartwright H, Halliday GM. Loss of thalamic intralaminar nuclei in progressive supranuclear palsy and Parkinson's disease: clinical and therapeutic implications. *Brain* 123: 1410–1421, 2000.

Herrero MT, Barcia C, Navarro JM. Functional anatomy of thalamus and basal ganglia. *Childs Nerv Syst* 8: 386–404, 2002.

Hille B. *Ion Channels of Excitable Membranes*. Sunderland, MA: Sinaur, 2001.

Hillman D, Chen S, Aung TT, Cherksey B, Sugimori M, Llinas RR. Localization of P-type calcium channels in the central nervous system. *Proc Natl Acad Sci USA* 88: 7076–7080, 1991.

Hobson JA, Pace-Schott EF. The cognitive neuroscience of sleep: neuronal systems, consciousness and learning. *Nat Rev Neurosci* 3: 679–693, 2002.

Iwasaki S, Takahashi T. Developmental changes in calcium channel types mediating synaptic transmission in rat auditory brainstem. *J Physiol* 509: 419–442, 1998.

Iwasaki S, Momiyama A, Uchitel OD, Takahashi T. Developmental changes in calcium channel types mediating central synaptic transmission. *J Neurosci* 20: 59–65, 2000.

Jeon D, Kim C, Yang YM, Rhim H, Yim E, Oh U, Shin HS. Impaired long-term memory and long-term potentiation in N-type Ca^{2+} channel deficient mice. *Genes Brain Behav* 4: 375–388, 2007.

Jones EG. Calcium channels in higher-level brain function. *Proc Natl Acad Sci USA* 104: 17903–17904, 2007.

Jouve L, Salin P, Melon P, Kerkerian-Le Goff L. Deep brain stimulation of the center median-parafascicular complex of the thalamus has efficient

anti-parkinsonian action associated with widespread cellular responses in the basal ganglia network in a rat model of Parkinson's disease. *J Neurosci* 29: 9919–9928, 2010.

Jouvet-Mounier D, Astic L, Lacote D. Ontogenesis of the states of sleep in rat, cat, and guinea pig during the first postnatal month. *Dev Psychobiol* 2: 216–239, 1970.

Katz B, Miledi R. The effect of calcium on acetylcholine release from motor nerve terminals. *Proc R Soc Lond B Biol Sci* 161: 483–495, 1965.

Kerkerian-Le Goff L, Bacci JJ, Jouve L, Melon C, Salin P. Impact of surgery targeting the caudal intralaminar thalamic nuclei on the pathophysiological functioning of basal ganglia in a rat model of Parkinson's disease. *Brain Res Bull* 2–3: 80–84, 2008.

Kezunovic N, Urbano FJ, Simon C, Hyde J, Smith K, Garcia-Rill E. Mechanism behind gamma band activity in pedunculopontine nucleus (PPN). *Eur J Neurosci* 34: 404–415, 2011.

Kha HT, Finkelstein DI, Pow DV, Lawrence AJ, Horne MK. Study of projections from the entopeduncular nucleus to the thalamus of the rat. *J Comp Neurol* 426: 366–377, 2000.

Kobayashi S, Nakamura Y. Synaptic organization of the rat parafascicular nucleus, with special reference to its afferents from the superior colliculus and the pedunculopontinetegmental nucleus. *Brain Res* 980: 80–91, 2003.

Le Van Quyen M, Staba A, Bragin A, Dixon C, Valderrama M, Fried I, Engel J. Large-scale microelectrode recordings of high-frequency gamma oscillations in human cortex during sleep. *J Neurosci* 30: 7770–7782, 2010.

Llinas RR. The intrinsic electrophysiological properties of mammalian neurons: insights into central nervous system function. *Science* 242: 1654–1664, 1988.

Llinas RR, Grace AA, Yarom Y. In vitro neurons in mammalian cortical layer 4 exhibit intrinsic oscillatory activity in the 10- to 50-Hz frequency range. *Proc Natl Acad Sci USA* 88: 897–901, 1991.

Llinas RR, Hess R. Tetrodotoxin-resistant dendritic spikes in avian Purkinje cells. *Proc Natl Acad Sci USA* 73: 2520–2523, 1976.

Llinas R., Leznik E, Urbano FJ. Temporal binding via cortical coincidence detection of specific and nonspecific thalamocortical inputs: a voltage-dependent dye-imaging study in mouse brain slices. *Proc Natl Acad Sci USA* 99: 449–454, 2002.

Llinas RR, Soonwook C, Urbano FJ, Hee-Sup S. γ-Band deficiency and abnormal thalamocortical activity in P/Q-type channel mutant mice. *Proc Natl Acad Sci USA* 104: 17819–17824, 2007.

Llinas RR, Steriade M. Bursting of thalamic neurons and states of vigilance. *J Neurophysiol* 95: 3297–3308, 2006.

Luo M, Perkel DJ. Long-range GABAergic projection in circuit essential for vocal learning. *J Comp Neurol* 403: 68–84, 1999.

McCormick DA. Cellular mechanisms underlying cholinergic and noradrenergic modulation of neuronal firing mode in the cat and guinea pig dorsal lateral geniculate nucleus. *J Neurosci* 12: 278–289, 1992.

Minamimoto T, Kimura M. Participation of the thalamic CM-Pf complex in attentional orienting. *J Neurophysiol* 87: 3090–3101, 2002.

Moruzzi G, Magoun HW. Brainstem reticular formation and activation. *Electroencephalogr Clin Neurophysiol* 1: 455–473, 1949.

Nelson MT, Todorovic SM, Perez-Reyes E. The role of T-type calcium channels in epilepsy and pain. *Curr Pharm Des* 12: 2189–2197, 2006.

Orieux G, Francois C, Fe'ger J, Yelnik J, Vila M, Ruberg M, Agid Y, Hirsch EC. Metabolic activity of excitatory parafascicular and pedunculopontine inputs to the subthalamic nucleus in a rat model of Parkinson's disease. *Neuroscience* 97: 79–88, 2000.

Parr-Brownlie LC, Poloskey SL, Bergstrom DA, Walters JR. Parafascicular thalamic nucleus activity in a rat model of Parkinson's disease. *Exp Neurol* 217: 269–281, 2009.

Pedroarena C, Llinas RR. Dendritic calcium conductances generate high-frequency oscillation in thalamocortical neurons. *Proc Natl Acad Sci USA* 94: 724–728, 1997.

Phelan KD, Mahler HR, Deere T, Cross CB, Good C, Garcia-Rill E. Postnatal maturational properties of rat parafascicular thalamic neurons recorded in vitro. *Thalamus Relat Syst* 1: 1–25, 2005.

Povysheva NV, Zaitsev A, Rotaru DC, Gonzales-Burgos G, Lewis DA, Krimer LS. Parvalbumin-positive basket interneurons in monkey and rat prefrontal cortex. *J Neurophysiol* 100: 2348–2360, 2008.

Raeva SN. The role of the parafascicular complex (CM-Pf) of the human thalamus in the neuronal mechanisms of selective attention. *Neurosci Behav Physiol* 36: 287–295, 2006.

Rhodes PA, Llinas RR. A model of thalamocortical relay cells. *J Physiol* 565: 765–781, 2005.

Simon C, Kezunovic N, Williams KD, Urbano FJ, Garcia-Rill E. Cholinergic and glutamatergic agonists induce gamma frequency activity in dorsal subcoeruleus nucleus neurons. *Am J Physiol Cell Physiol* 301: C327–C335, 2011.

Simon C, Kezunovic N, Ye M, Hyde J, Hayar A, Williams DK, Garcia-Rill E. Gamma band unit and population responses in the pedunculopontine nucleus. *J Neurophysiol* 104: 463–474, 2010.

Steriade M, Datta S, Pare D, Oakson G, CurroDossi RC. Neuronal activities in brain-stem cholinergic nuclei related to tonic activation processes in thalamocortical systems. *J Neurosci* 10: 2541–2559, 1990.

Steriade M, Demetrescu M. Unspecific systems of inhibition and facilitation of potentials evoked by intermittent light. *J Neurophysiol* 23: 602–617, 1960.

Steriade M, McCormick DA, Sejnowski TJ. Thalamocortical oscillations in the sleeping and aroused brain. *Science* 262: 679–685, 1993.

Sterin-Borda L, Ganzinelli S, Berra A, Borda E. Novel insight into the mechanisms involved in the regulation of the m1 muscarinic receptor, iNOS and nNOS mRNA levels. *Neuropharmacology* 45: 260–269, 2003.

Uchitel OD, Protti DA, Sanchez V, Cherkesey BD, Sugimori M, Llinas RR. P-type voltage-dependent calcium channel mediates presynaptic calcium influx and transmitter release in mammalian synapses. *Proc Natl Acad Sci USA* 89: 3330–3333, 1992.

Van der Werf YD, Witter MP, Groenewegen HJ. The intralaminar and midline nuclei of the thalamus. Anatomical and functional evidence for participation in processes of arousal and awareness. *Brain Res* 39: 107–140, 2002.

Vanderwolf CH. What is the significance of gamma wave activity in the pyriform cortex? *Brain Res* 877: 125–133, 2000.

Von der Kammer H, Demiralay C, Andresen B, Albrecht C, Mayhaus M, Nitsch R. Regulation of gene expression by muscarinic acetylcholine receptors. *Biochem Soc Symp* 67: 131–140, 2001.

Watson RT, Heilman KM, Miller BD, King FA. Neglect after mesencephalic reticular formation lesions. *Neurol* 24: 294–298, 1974.

Williams JA, Comisarow J, Day J, Fibiger HC, Reiner PB. State-dependent release of acetylcholine in rat thalamus measured by in vivo microdialysis. *J Neurosci* 14: 5236–5242, 1994.

Ye M, Hayar A, Garcia-Rill E. Cholinergic responses and intrinsic membrane properties of developing thalamic parafascicular neurons. *J Neurophysiol* 2: 774–785, 2009.

Zhang L, Renaud L, Kolaj M. Properties of T-type Ca^{2+} channel-activated slow afterhyperpolarization thalamic paraventricular nucleus and other thalamic midline neurons. *J Neurophysiol* 101: 2741–2750, 2009.

Zhou L, Gall D, Qu Y, Prigogine C, Cheron G, Tissir F, Schiffmann SN, Goffinet A. Maturation of "Neocortex Isole" in vivo in mice. *J Neurosci* 30: 7928–7939, 2010.